



Measurement-induced phase transitions by matrix product states scaling

Guillaume Cecile , Hugo Lóio , and Jacopo De Nardis

Laboratoire de Physique Théorique et Modélisation, CNRS UMR 8089, CY Cergy Paris Université, 95302 Cergy-Pontoise Cedex, France

 (Received 18 March 2024; accepted 5 June 2024; published 26 August 2024)

We study the time evolution of long quantum spin chains subjected to continuous monitoring projected on matrix product states (MPS) with fixed bond dimension, by means of the Time-Dependent Variational Principle (TDVP) algorithm. The latter gives an effective unitary evolution which approximates the real quantum evolution up to the projection error. We show that such error displays, at large times, a phase transition in the monitoring strength, which can be well detected by scaling analysis with relatively low values of bond dimensions. Moreover, in the presence of $U(1)$ global spin charge, we show the existence of a charge-sharpening transition well separated from the entanglement transition which we detect by studying the charge fluctuations of a local subpart of the system at large times. Our work shows that quantum monitored dynamics projected on MPS manifolds contains relevant information on measurement-induced phase transitions and provides a new method to identify measured-induced phase transitions in systems of arbitrary dimensions and sizes.

DOI: [10.1103/PhysRevResearch.6.033220](https://doi.org/10.1103/PhysRevResearch.6.033220)

I. INTRODUCTION

The dynamics of quantum many-body systems are particularly challenging due to the rapid growth of entanglement throughout the system. Indeed, even if the initial state is a simple product state, unitary time evolution typically entangles the different degrees of freedom in the system [1,2], and the wave function rapidly becomes exponentially complex. This picture is challenged when on top of the unitary dynamics one adds an externally induced non-Hermitian contribution to the evolution, for example, when the system is continuously monitored or measured at a given rate γ [3–10]. In this case, the average von Neumann entanglement entropy of the system transits from a volume law scaling to an area law, depending on the rate of monitoring. Such a phase transition has been dubbed measured-induced phase transition (MIPT) and has received a large experimental and theoretical attention in the past years due to its numerous and inspiring connections with quantum computing and error correction theory (e.g., [3–5,11–70]).

Here we aim to detect MIPT as a simulability transition by tensor network wave functions (see also, e.g., [65,71–73]). We consider matrix product states (MPS), which are well-known efficient representations of any wave function with area law entanglement scaling, [74–76]: that is, given the bond dimension of the MPS χ , one expects that an MPS wave function can represent any area law wave functions only up to exponentially small (in bond dimension χ) corrections. Doing time evolution with MPS methods is instead challenging, as the spread of entanglement throughout the system makes

their bond dimension grow, typically exponentially with time. However, in the presence of strong monitoring, the bond dimension is expected to saturate at large times, signaling this way the emerging area law phase.

Partially motivated by ideas of hydrodynamics, where classical nonlinear dynamics with the necessary conservation

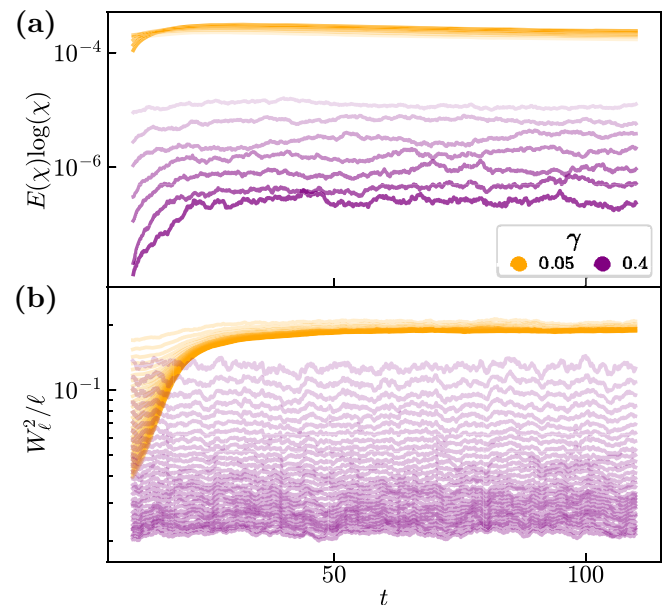


FIG. 1. Monitored XXX chain initialized in the Néel state. (a) Time evolution of the error rate multiplied by $\log \chi$ with TDVP evolution of a chain with $L = 60$ sites with different values of $\chi = n^2$, $n \in [4, 10]$ (light to dark shades of color) and with two values of γ , one in the volume law phase and one in the area law phase. (b) Same for the charge fluctuations on subsystems of size ℓ with different $\ell \in [2, 30]$.

Published by the American Physical Society under the terms of the [Creative Commons Attribution 4.0 International license](https://creativecommons.org/licenses/by/4.0/). Further distribution of this work must maintain attribution to the author(s) and the published article's title, journal citation, and DOI.

laws well reproduce large-scale proprieties, here we consider the time evolution of MPS with fixed bond dimension as given by the Time-Dependent Variational Principle (TDVP) [66,71,77–82]. Here, the Hamiltonian time evolution at each time step is projected back on the manifold of MPS with fixed bond dimensions χ . Such evolution is known to conserve total energy and any other local conserved charge, such as total magnetization. Moreover, the TDVP time evolution, as the projection is state dependent, is a *unitary, nonlinear* evolution, as opposed to other methods for MPS evolution. Therefore, the average of monitored projected trajectories is expected to be much different from the average state. Here we show that finite- χ scalings of the transition are very well present in this effective projected quantum evolution. When projecting the unitary time evolution of a Hamiltonian into the space of MPS with bond dimension χ , the norm of the orthogonal vector to the space at any time step gives a measure of the distance between the true quantum evolution and the projected one. As the maximal entanglement entropy contained in an MPS is $\log \chi$, such *error rate* (time averaged over long time scales) decays as $1/\log \chi$ for unitary evolution. Here we show that this scaling changes drastically as the monitoring rate is increased, transmuting to exponential decay, for $\gamma > \gamma_c$. This transition, which remarkably can be already found within the variational space of MPS wave functions, we conjecture to be the same as the entanglement transition, and we characterize by employing a rescaling in bond dimension χ . By involving relatively small values of bond dimensions and with no limits in the system size, we can therefore access the MIPT in regimes which would be impossible for other numerical methods. Analogously to the equilibrium case (see, in particular, [83–86]), where the finite bond dimension introduces an effective length $L(\chi) \sim \chi^\kappa$, and where scaling in bond dimension can be usefully used to probe critical phenomena, our approach extends these ideas to the study of MIPTs.

Moreover, given that the TDVP evolution preserves the eventual global $U(1)$ symmetry of the Hamiltonian, we employ a scaling to study the charge-sharpening (CS) transition, which is conjectured to occur at smaller measurement rates compared to the entanglement transition [87–90]. To extend the CS protocol to large system sizes, here we consider the variance of the fluctuations of the local magnetization on a subsystem of size ℓ . For example, by defining $Q_\ell = \sum_{j \in \ell} S_j^z$,

we introduce its variance as

$$W_\ell^2 = \langle Q_\ell^2 \rangle - \langle Q_\ell \rangle^2 = \sum_{i,j \in \ell} \langle S_i^z S_j^z \rangle^c, \quad (1)$$

averaged over quantum trajectories (as for all other quantities we compute), and we show that the latter shows a transition at large times from an ETH-like extensive behavior $W_\ell^2 \sim \ell$ [90–92] to a subextensive one $W_\ell^2 \sim \ell^\alpha$ with $\alpha < 1$, for $\gamma \geq \gamma_\#$. We stress that a subextensive variance signals a form of anticorrelated connected spin-spin correlations, and one can also find subextensive fluctuations with purely unitary evolution in some particular cases [93] or in Luttinger liquid ground states, where $W_\ell^2 \sim \ell^0$. We find that for any given $\chi \gtrsim 16$, the data can be rescaled well on a piece-wise function such that $f(\gamma - \gamma_\#)$ for $\gamma < \gamma_\#$ and $f(\log \ell(\gamma - \gamma_\#))$ for $\gamma > \gamma_\#$, in perfect agreement with the predicted Kosterlitz-Thouless (KT) scaling [89] (which represents its first clear observation in a experimentally relevant system). As the fitted $\gamma_\#$ is converged already at small values of bond dimension, we find, in all cases studied, that such transition always appears at a smaller rate than the MIPT $\gamma_\# < \gamma_c$.

II. MODELS AND METHODS

We focus on two generic interacting systems in one dimension (whose MIPT has been also studied by different means also in Refs. [19,94,95]), namely, a chain of L spin-1/2 particles, unitarily evolving with $U(1)$ symmetric (magnetization-conserving) Hamiltonians, defined as

$$\hat{H}_{J\text{-XXX}} = \sum_{i=1}^L (\hat{S}_i^x \hat{S}_{i+1}^x + \hat{S}_i^y \hat{S}_{i+1}^y + \hat{S}_i^z \hat{S}_{i+1}^z) + \sum_{i=1}^L J(\hat{S}_i^x \hat{S}_{i+2}^x + \hat{S}_i^y \hat{S}_{i+2}^y), \quad (2)$$

with spin operators \hat{S}_i^α and with $J = 0$ (XXX chain) or $J = 1/2$ (J-XXX chain). In addition to unitary evolution, the systems evolve under continuous weak monitoring of the local spin operator \hat{S}_i^z , for each site i with a rate of measurement γ . The associated monitored dynamics of the quantum state are described by the following stochastic Schrödödinger equation (SSE) [96–98] for the many-body state $|\psi\rangle$,

$$d|\psi_t\rangle = -iHdt|\psi_t\rangle + \sum_{i=1}^L \left[\sqrt{\gamma}(\hat{S}_i^z - \langle \hat{S}_i^z \rangle_t) dW_t^i - \frac{\gamma}{2} (\hat{S}_i^z - \langle \hat{S}_i^z \rangle_t)^2 dt \right] |\psi_t\rangle, \quad (3)$$

with the expectation value of the local magnetization given by the state at a given time $\langle \hat{S}_i^z \rangle_t = \langle \psi_t | \hat{S}_i^z | \psi_t \rangle$. Equation (3) can be easily simulated by alternating its unitary and measurement terms via a Trotter splitting,

$$|\psi_{t+\delta t}\rangle \approx C e^{\sum_{j=1}^L [\delta W_j^i + 2\langle \hat{S}_j^z \rangle_{t+\delta t} \delta S_j^z]} e^{-i\hat{H}\delta t} |\psi_t\rangle, \quad (4)$$

where the set of δW^i are generated each time step from a normal distribution with variance $\sqrt{\gamma\delta t}$ and zero mean and C is a normalizing constant. As the measurements are only made by single site operators, they do not require any TDVP

projection on the space of MPS, differently from the unitary part, as we shall now describe. We begin by expressing the wavefunction $|\Psi(M)\rangle$ as an MPS made up of the set of tensors $\{M\}$ each with a local basis $\{|\sigma_i\rangle\}_{\sigma_i=1}^{d_i}$ and bond dimensions $\{\chi_i\}$,

$$|\Psi(M)\rangle = \sum_{\sigma_1, \dots, \sigma_L} M_{1;\chi_1}^{\sigma_1} \cdots M_{L;\chi_{L-1}}^{\sigma_L} |\sigma_1 \cdots \sigma_L\rangle, \quad (5)$$

where in the following we always refer to χ as the maximal value of the set $\{\chi_i\}$. Typically, time evolution of MPS is

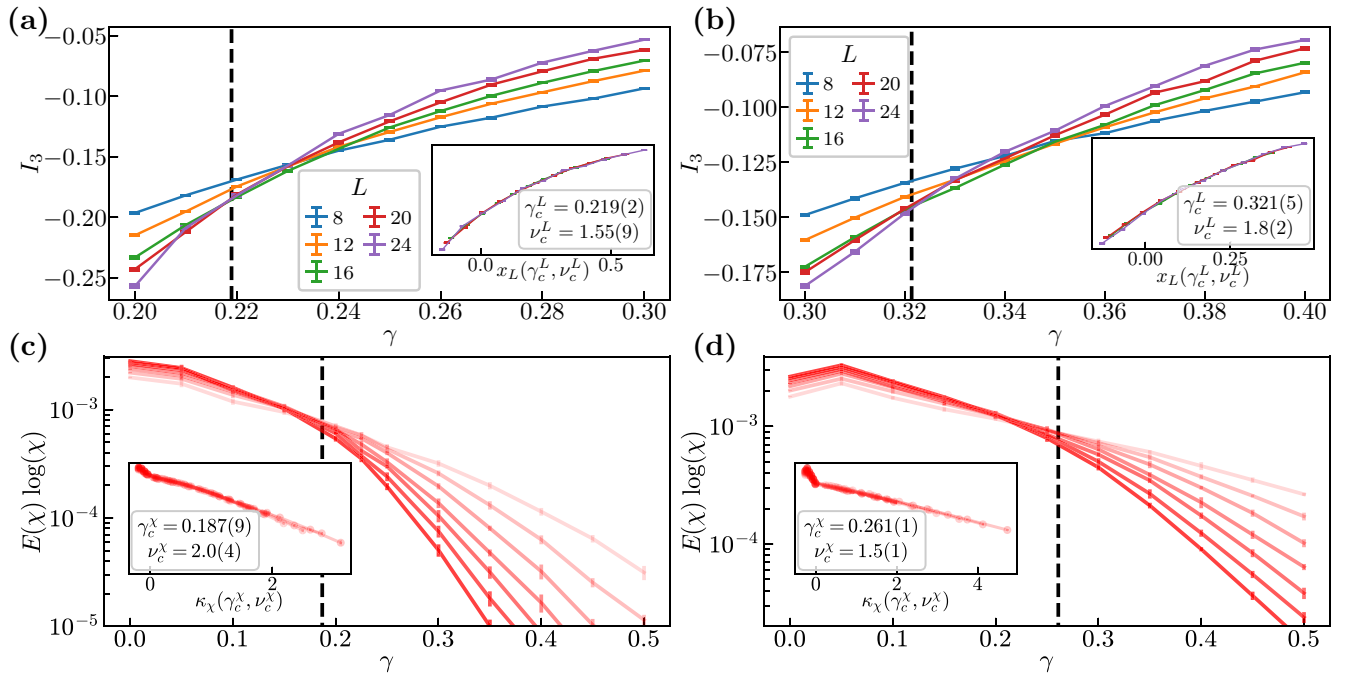


FIG. 2. Entanglement/Error phase transitions in the XXX model, (a) and (c), and in the J-XXX model, (b) and (d). Dashed vertical lines correspond to the extracted critical measurement rates. (a), (b) Tripartite mutual information I_3 from ED simulations, time averaged for $t \in [2L, 4L]$, as a function of measurement rate γ for several sizes L . Inset: Data collapse for $L \geq 16$. (c), (d) In semi-log scale, the projection error multiplied by $\log(\chi)$ obtained from the TDVP algorithm as a function of measurement rate γ for $\chi = n^2$ for $n \in [2, 10]$ (from light to dark shades of red) with dashed vertical lines corresponding to γ_c in the inset. Insets: Data collapsed obtained from finite scaling analysis for $\chi = n^2$ for $n \in [4, 10]$ (same color code) with corresponding critical parameters with additional data points around transition.

carried by methods such as TEBD [99], where two or higher body gates are applied and entanglement is created between adjacent sites. However, this gives an effective nonlinear time evolution when truncating the entanglement to a fixed maximal value. Another approach is to fix a maximal bond dimension $\chi_i = \chi$ and then time evolve the MPS such that at each time step the evolution is projected back on the manifold of MPS with that given bond dimension. This is achieved by introducing a projector $P_{\mathcal{T}_M \mathcal{M}}$ which projects onto the tangent space of the state $|\Psi(M)\rangle$ with fixed bond dimension χ , at any time t , resulting in the TDVP time evolution

$$i\partial_t |\Psi(M)\rangle = P_{\mathcal{T}_M \mathcal{M}} \hat{H} |\Psi(M)\rangle. \quad (6)$$

Projecting to the manifold of fixed bond dimension leads to a projection error $|\phi\rangle = \hat{H} |\Psi(M)\rangle - P_{\mathcal{T}_M \mathcal{M}} \hat{H} |\Psi(M)\rangle$, representing the orthogonal state to the local manifold of MPS. In our analysis, we define the norm of this residue as the projection error rate. Given the projector $P_\psi(M_\chi)$ on the manifold of bond dimension χ , the projection error rate is given by

$$E(\chi) = \|\hat{H} |\psi\rangle - P_\psi(M_\chi) \hat{H} |\psi\rangle\|^2, \quad (7)$$

which can be easily evaluated [77,78,100] and where, most importantly, it can be decomposed in terms of L local terms. We remark that, since the projector depends on the state itself (in particular, on two copies of the state), this expression is nonlinear in the density matrix $\rho = |\psi\rangle \langle \psi|$, therefore making it a good quantity to detect MIPT.

To benchmark the TDVP data, we also implement exact diagonalization (ED) simulations, where one can probe the tripartite mutual information I_3 [46] and detect the entanglement transition from the crossing of I_3 (obtained by partitioning the system into three parts of equal lengths) for different L s as function of γ . To find the correct critical parameters for the transitions, a finite-size scaling analysis of a given observable \mathcal{O} is performed with $\mathcal{O}(\gamma, A) \sim f[x(\gamma, \gamma_{\mathcal{O}}, A), \nu_{\mathcal{O}}]$, where A corresponds to either L , in the case of ED simulations, or χ in the case of TDVP, and x is an appropriate scaling function. The standard ansatz for the scaling function is $x = x_A(\gamma_{\mathcal{O}}, \nu_{\mathcal{O}}) = (\gamma - \gamma_{\mathcal{O}})A^{1/\nu_{\mathcal{O}}}$ together with the logarithmic (KT) scaling in A in the limit $\nu_{\mathcal{O}} \rightarrow \infty$, $x = x_A(\gamma_{\mathcal{O}}, \infty) = (\gamma - \gamma_{\mathcal{O}}) \log(A)$. To fit the MPS transition, given the much quicker convergence in χ on the left of the critical point (see Fig. 2), we need to introduce a *piece-wise ansatz*, namely

$$x = \kappa_A(\gamma_{\mathcal{O}}, \nu_{\mathcal{O}}) = \begin{cases} (\gamma - \gamma_{\mathcal{O}}) & \gamma < \gamma_{\mathcal{O}} \\ (\gamma - \gamma_{\mathcal{O}})A^{1/\nu_{\mathcal{O}}} & \gamma > \gamma_{\mathcal{O}} \end{cases}, \quad (8)$$

and we cross checked this scaling with the one where only the right side of the transition is fitted, giving analogous results. When $\mathcal{O}(\gamma, A)$ probes the MIPT, then $\gamma_{\mathcal{O}} = \gamma_c^A$ and $\nu_{\mathcal{O}} = \nu_c^A$, else if the CS is probed, $\gamma_{\mathcal{O}} = \gamma_{\#}^A$ and $\nu_{\mathcal{O}} = \nu_{\#}^A$. We refer the reader to the Appendixes for more details on the fitting procedure.

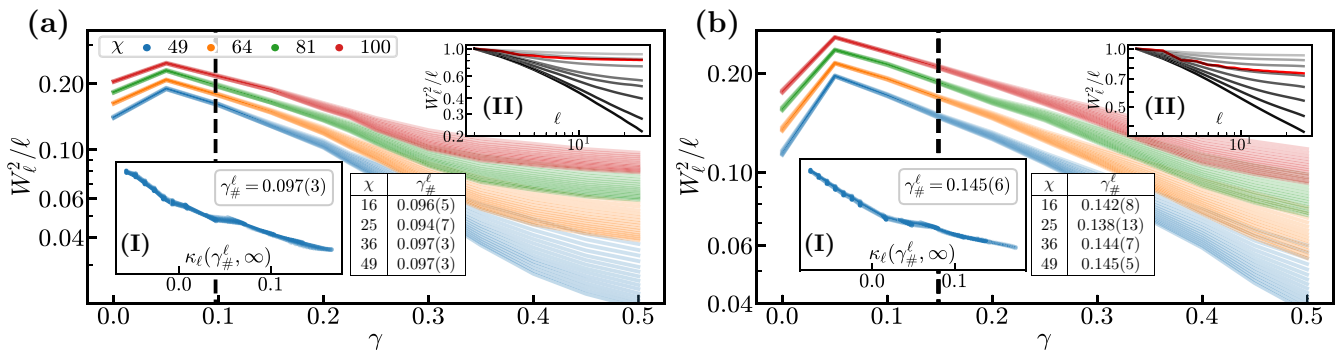


FIG. 3. CS phase transitions for (a) the XXX model and (b) the J-XXX model. Dashed vertical lines correspond to the extracted critical rates. Main plots: In semi-log scale, magnetization variance divided by ℓ shifted by 0.02 for each different χ s (to increase readability) and for increasing $\ell \in [2, 25]$ (light to dark shades of colors); the dashed vertical line corresponds to $\gamma_{\#}$ from the inset. Insets(I) data collapsed for $\chi = 49$ with corresponding $\gamma_{\#}$. Insets(II), shown in log-log scale, W_{ℓ}^2/ℓ as a function of ℓ for $\gamma = 0.05 n$ with $n \in [0, 10]$ (light to dark shades of gray with $\gamma = 0$ shown in red) for $\chi = 100$. The inset tables show the extracted values of the critical transition rate (with KT scaling) at different values of χ .

III. RESULTS AND DISCUSSION

Starting always with the initial Néel state, $|\Psi(0)\rangle = |\downarrow\uparrow\downarrow\uparrow \dots \downarrow\uparrow\rangle$, we perform monitored evolution at different values of χ . In Fig. 1, we show the time evolution of the error rate for two different values of γ to illustrate how after a time scale of order L the latter saturates to a steady value, which we plot as a function of χ in Fig. 2. As expected for the volume law phase, at lower γ , $E(\chi)\log(\chi)$ converges to a constant value in χ at large χ for fixed $\gamma < \gamma_c$. By increasing γ , we observe a transition to a regime where the error decays exponentially with χ , corresponding to the area law phase. The existence of a transition can also be verified by ED simulations. There, a crossing in I_3 as a function of γ for different values of L allows for the identification of the transition. In both cases, the critical parameters are precisely found by a scaling analysis which reveals how MPS scaling determines a critical measurement rate γ_c^{χ} quite smaller than that of the ED, γ_c^L . Indeed, it is expected that the critical measurement rates obtained in a small system L drift *toward the left* with increasing L , as a smaller circuit is easier to volume law entangle (which is visible also from Figs. 2(a) and 2(b)). The unitary (entangling) terms tend to dominate over measurements for small L , an effect which is indeed more prominent in the (longer range) J-XXX model. The extracted γ_c^{χ} instead does not suffer from finite L corrections as the system here is large enough ($L = 60$ in all data presented here, and we have checked that different values of $L \geq 40$ give the same results), but it could in principle suffer from finite χ effects, which should instead cause a drift of the critical γ *toward the right*, as larger values of χ allow for more entanglement in the MPS. However, we find it very well converged already for relatively small values of bond dimension. For the XXX chain, the critical value $\gamma_c \simeq 0.19$ has been already found by different MPS-based methods in Ref. [94], and it is indeed much smaller than the value predicted by ED with $L \leq 24$, $\gamma_c^L \simeq 0.22$.

The two extracted critical exponents also slightly differ between ED and MPS, but in general, they are expected to do so. Indeed, for pure states, a finite χ typically translates into

a finite effective correlation length $L(\chi) \sim \chi^{\kappa}$ [83–86], with therefore a factor κ between L -scaling and χ -scaling. While the latter is indeed well established for equilibrium ground states, much less is known for nonequilibrium settings.

Moving to the CS transition, we extract the late time value of the variance, and we plot it in Fig. 3. For small γ , W_{ℓ}^2/ℓ converges to a constant (γ, χ) (which, quite remarkably, is not a monotonous function γ) at large ℓ , for fixed $\gamma < \gamma_{\#}$ and any χ , meaning that the charge fluctuations are extensive in the subsystem size ℓ . When $\gamma = 0$, this scaling is expected by ETH-like arguments, as the system thermalizes locally to a canonical state within the MPS manifold. Increasing γ enough, one encounters a transition to a phase where W_{ℓ}^2 scales sublinearly. Once again, we observe that such behavior converges very fast with bond dimension. Using a KT piecewise scaling, we can fix the critical $\gamma_{\#}$, which we find again slightly smaller than the ones predicted by ED simulations (see the Appendixes), where the difference is again imputable to finite L effects. Finally, we remark that our findings are only partially in agreement with the theory carried for a random circuit with large qudits [89]: despite the agreement on the predicted KT scaling, we find a transition from extensive to subextensive variance (as also observed in Ref. [90] in small systems), where in Ref. [89] the transition is between an extended critical $\log \ell$ scaling for $0 < \gamma < \gamma_{\#}$ and a subextensive scaling phase. The differences could be imputable to either deviations from the theory, due to small/intermediate-scale physics, or to the TDVP effective classical dynamics used here. However, by cross checking with ED simulations, here we provide strong evidence that the transition observed must be the same, even if the scaling of the variance in the two phases is apparently different. We shall leave this interesting question to further studies, yet we stress the importance of methods such as the one proposed here to probe the CS transition in large systems with continuous time.

IV. CONCLUSION

Our work shows the surprising fact that monitored dynamics at large times *within the MPS manifolds at fixed χ*

already contains information about MIPT and CS transitions. Therefore, besides introducing new tractable numerical ways to estimate critical parameters of MIPT in large systems, we show that MIPT can also be seen as transitions directly inside manifolds of variational states rather than on the whole Hilbert space. We have found a transition in the error rate at large times, of the TDVP, directly related to the entanglement transition. We stress that the fact that such transition exists is far from obvious: indeed, MPS can simulate quantum evolution correctly only by taking the limit $\chi \rightarrow \infty$ first, then $t \rightarrow \infty$ (at least in the volume law phase). Here we show that, remarkably, by reversing the two limits, the MIPT and CS can still be detected. Moreover, the relatively quick convergence in χ could be understood from the fact that an ensemble of MPSs can successfully incorporate short (quantum-like) and long (classical-like) fluctuations (see [101,102]). As MIPTs probe the properties of the ensemble of quantum trajectories, it is reasonable that many of its features are already visible by an ensemble of MPS with relatively small bond dimensions, enough to incorporate the leading quantum effects. It therefore remains a lingering question to better clarify the scaling with χ , as done for equilibrium critical states, and to employ our method, for example, to access MIPTs in higher dimensions. It will also be interesting to study more closely monitored TDVP evolution at small values of bond dimension as done for quantum scars dynamics [103,104].

Finally, we remark that our approach directly gives new useful insights to circumvent the well-known postselection problem [65,105,106], namely the exponential complexity of measuring the entanglement entropy a single quantum trajectory. Given the optimal performance of the scalings shown here, it is clear that the distance of Eq. (7), between the exact state $|\psi\rangle$ (obtained by an exact quantum simulation) and its projected state $|\psi_{M_\chi}\rangle$ (classically computed by evolving the state on the manifold at fixed χ with the same measurements outputs) on the MPS manifold with bond dimension χ , namely the observable

$$E(\chi) = 1 - \langle \psi | \psi_{M_\chi} \rangle, \quad (9)$$

can be effectively computed on each quantum trajectory $|\psi\rangle$, and by rescaling in χ , analogously to what is done in Fig. 2, one can get access to most of the MIPT critical parameters. We shall return to this exiting application in the near future.

ACKNOWLEDGMENTS

We are extremely grateful to Xhek Turkeshi for enlightening discussions, help with different technical aspects, and valuable feedback. We also thank Romain Vasseur, Adam Nahum, Andrea De Luca, Silvia Pappalardi, Michael Buchhold, Guglielmo Lami, Mario Collura, Luca Lumia, Laurens Vanderstraeten, and Jutho Haegeman for discussions. This work was partially funded by ERC Starting Grants No. 101042293 (HEPIQ) and No. ANR-22-CPJ1-0021-01. The work was granted access to the HPC resources of IDRIS under the allocations Grants No. AD010513967R1 and No. A0140914149 and with an MPS code developed using the C++ + iTensor library [107].

APPENDIX A: CS TRANSITION IN ED SIMULATIONS

To probe the CS transition, the initial state is chosen to be in a superposition of states in all possible charge sectors,

$$|\Psi(0)\rangle = \bigotimes_{i=1}^L (|\uparrow\rangle + |\downarrow\rangle). \quad (A1)$$

For the time evolution, we employ a first-order Trotterization protocol to separate the unitary evolution operator into layers of commuting 2-qubit gates. In the case of the XXX model, the time evolution operator for a single step is given by

$$\hat{U}_{\text{XXX}} \approx \prod_i \hat{u}_{2i,2i+1}^{\text{XXX}} \prod_i \hat{u}_{2i-1,2i}^{\text{XXX}}, \quad (A2)$$

with an odd followed by an even layer of 2-qubit gates

$$\hat{u}_{i,i+1}^{\text{XXX}} = \exp \left[-i\delta t (\hat{S}_i^x \hat{S}_{i+1}^x + \hat{S}_i^y \hat{S}_{i+1}^y + \hat{S}_i^z \hat{S}_{i+1}^z) \right], \quad (A3)$$

where $\delta t \ll 1$. In the case of the J-XXX model, we apply the same evolution operator of the XXX model followed by a dense arrangement in three layers of all possible 2-qubit gates

$$\hat{u}_{i,i+2}^J = \exp \left[-i\delta t J (\hat{S}_i^x \hat{S}_{i+2}^x + \hat{S}_i^y \hat{S}_{i+2}^y) \right]. \quad (A4)$$

To implement the measurements, a strong measurement procedure was employed. With probability $p = \gamma\delta t$, each site i is measured according to the Born rule,

$$|\psi\rangle \rightarrow P_\pm |\psi\rangle, \quad P_\pm = \left(\frac{\mathbb{1}}{2} \pm \hat{S}_i^z \right), \quad (A5)$$

where P_\pm is the projector or Kraus operator corresponding to \hat{S}_i^z and + or - is chosen with corresponding probability $p_\pm = \langle \psi | P_\pm | \psi \rangle$.

Apart from the initial state, the simulations of Figs. 2(a) and 2(b) follow the same protocol. However, since the models are $U(1)$ conserving, meaning all 2-qubit gates are block diagonalized as

$$\hat{u} = \begin{pmatrix} \hat{u}_{1 \times 1} & & \\ & \hat{u}_{2 \times 2} & \\ & & \hat{u}_{1 \times 1} \end{pmatrix}, \quad (A6)$$

if the initial conditions are such that we are bound to a single sector of the Hilbert space, then we need not simulate the other sectors. Taking these symmetry considerations into account is important to perform more efficient simulations and reach larger system sizes and sampling pools [108].

The measurements will eventually collapse the state of Eq. (A1) into a single sector, which can happen at different time scales, depending on γ . For $\gamma < \gamma_\#$, the time scale is $\mathcal{O}(L)$, whereas for $\gamma > \gamma_\#$, it is sublinear in system size [87]. At any time, the spread of the active sectors is given by the variance

$$W^2(t) = \langle Q^2(t) \rangle - \langle Q(t) \rangle^2, \quad (A7)$$

where, for the total magnetization of the system, we drop the label ℓ in Eq. (1), meaning $\ell = L$.

Due to the change in CS time scales, a crossing of W^2 at $t \propto L$ is observed at the critical measurement rate (Fig. 4). Analogously to the main text, we find that $\gamma_\#^L = 0.151(2)$ for the XXX model in Fig. 4(a) is smaller than that of the J-XXX

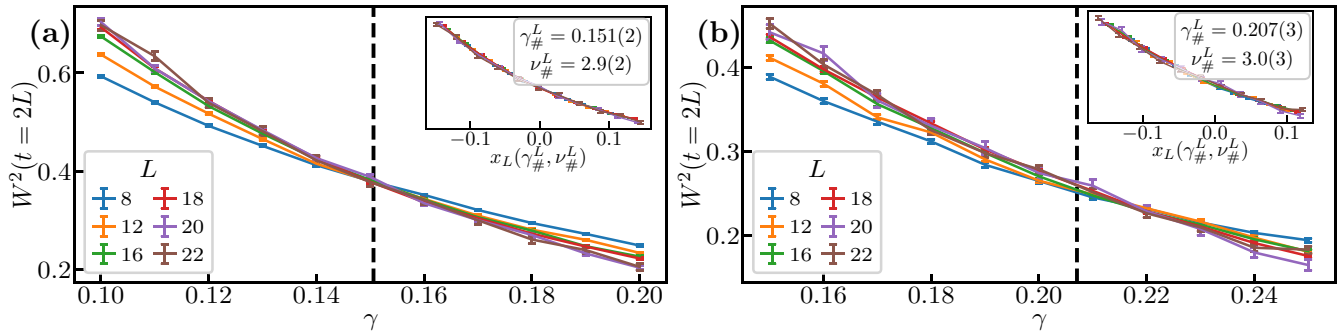


FIG. 4. Magnetization variance W^2 at time $t = 2L$ for (a) the XXX model and (b) the J-XXX model, as a function of γ for different L . Dashed vertical lines correspond to critical measurement rates. Insets: data collapse and corresponding critical parameters.

model, $\gamma_{\#}^L = 0.207(3)$, in Fig. 4(b). These critical measurement rates are larger than corresponding ones found with the TDVP method (see Fig. 3), reflecting the phenomenology already found in the entanglement/error transition.

APPENDIX B: DESCRIPTION OF THE FITTING ALGORITHM

The correct critical parameters for the scaling functions are the ones that minimize the cost function [46,109,110]

$$\begin{aligned}
 W(\gamma_{\mathcal{O}}, \nu_{\mathcal{O}}) &= \frac{1}{n-2} \sum_{i=2}^{n-1} w(x_i, y_i, d_i | x_{i-1}, y_{i-1}, d_{i-1}, x_{i+1}, y_{i+1}, d_{i+1}), \\
 &\quad (B1)
 \end{aligned}$$

where $x_i = x(\gamma_i, \gamma_{\mathcal{O}}, A_i, \nu_{\mathcal{O}}^A)$ is the scaling function value of the i th data point of a total of n data points, sorted such

that $x_{i+1} \geq x_i$, with values $y_i = \mathcal{O}(\gamma_i, A_i)$ and corresponding errors d_i . The cost density is given by $w(x_i, y_i, d_i | \dots) = (y_i - \bar{y})^2 / \Delta$, with

$$\begin{aligned}
 \bar{y} &= \frac{(x_{i+1} - x_i)y_{i-1} - (x_{i-1} - x_i)y_{i+1}}{x_{i+1} - x_{i-1}} \\
 \Delta &= d_i^2 + \left(\frac{x_{i+1} - x_i}{x_{i+1} - x_{i-1}} d_{i-1} \right)^2 + \left(\frac{x_{i-1} - x_i}{x_{i+1} - x_{i-1}} d_{i+1} \right)^2.
 \end{aligned}$$

If $x_{i-1} = x_{i+1}$ (which happens with the κ_A scaling function), we get undefined 0/0 terms in the cost density, which we resolve by taking the limit where x_i sits precisely in the midpoint between x_{i-1} and x_{i+1} as they approach each other. This cost function works by minimizing the distance from y_i to the line determined by the points at $i-1$ and $i+1$, consequently locally aligning the points.

-
- [1] A. P. Luca D'Alessio, Yariv Kafri, and M. Rigol, From quantum chaos and eigenstate thermalization to statistical mechanics and thermodynamics, *Adv. Phys.* **65**, 239 (2016).
- [2] A. Nahum, J. Ruhman, S. Vijay, and J. Haah, Quantum entanglement growth under random unitary dynamics, *Phys. Rev. X* **7**, 031016 (2017).
- [3] Y. Li, X. Chen, and M. P. A. Fisher, Measurement-driven entanglement transition in hybrid quantum circuits, *Phys. Rev. B* **100**, 134306 (2019).
- [4] A. Chan, R. M. Nandkishore, M. Pretko, and G. Smith, Unitary-projective entanglement dynamics, *Phys. Rev. B* **99**, 224307 (2019).
- [5] B. Skinner, J. Ruhman, and A. Nahum, Measurement-induced phase transitions in the dynamics of entanglement, *Phys. Rev. X* **9**, 031009 (2019).
- [6] R. Vijay, C. Macklin, D. H. Slichter, S. J. Weber, K. W. Murch, R. Naik, A. N. Korotkov, and I. Siddiqi, Stabilizing Rabi oscillations in a superconducting qubit using quantumfeedback, *Nature (London)* **490**, 77 (2012).
- [7] N. Katz, M. Ansmann, R. C. Bialczak, E. Lucero, R. McDermott, M. Neeley, M. Steffen, E. M. Weig, A. N. Cleland, J. M. Martinis, and A. N. Korotkov, Coherent state evolution in a superconducting qubit from partial-collapse measurement, *Science* **312**, 1498 (2006).
- [8] P. Campagne-Ibarcq, P. Six, L. Bretheau, A. Sarlette, M. Mirrahimi, P. Rouchon, and B. Huard, Observing quantum state diffusion by heterodyne detection of fluorescence, *Phys. Rev. X* **6**, 011002 (2016).
- [9] M. Bauer, D. Bernard, and A. Tilloy, Computing the rates of measurement-induced quantum jumps, *J. Phys. A: Math. Theor.* **48**, 25FT02 (2015).
- [10] F. Carollo and V. Alba, Entangled multiplets and spreading of quantum correlations in a continuously monitored tight-binding chain, *Phys. Rev. B* **106**, L220304 (2022).
- [11] A. Nahum, S. Roy, B. Skinner, and J. Ruhman, Measurement and entanglement phase transitions in all-to-all quantum circuits, on quantum trees, and in Landau-Ginsburg theory, *PRX Quantum* **2**, 010352 (2021).
- [12] C.-M. Jian, Y.-Z. You, R. Vasseur, and A. W. W. Ludwig, Measurement-induced criticality in random quantum circuits, *Phys. Rev. B* **101**, 104302 (2020).
- [13] X. Cao, A. Tilloy, and A. De Luca, Entanglement in a fermion chain under continuous monitoring, *SciPost Phys.* **7**, 024 (2019).

- [14] A. C. Potter and R. Vasseur, Entanglement dynamics in hybrid quantum circuits, in *Entanglement in Spin Chains: From Theory to Quantum Technology Applications*, edited by A. Bayat, S. Bose, and H. Johannesson (Springer, Cham, 2022), pp. 211–249.
- [15] S. Czischek, G. Torlai, S. Ray, R. Islam, and R. G. Melko, Simulating a measurement-induced phase transition for trapped-ion circuits, *Phys. Rev. A* **104**, 062405 (2021).
- [16] Y. Han and X. Chen, Entanglement structure in the volume-law phase of hybrid quantum automaton circuits, *Phys. Rev. B* **107**, 014306 (2023).
- [17] Y. Minoguchi, P. Rabl, and M. Buchhold, Continuous Gaussian measurements of the free boson CFT: A model for exactly solvable and detectable measurement-induced dynamics, *SciPost Phys.* **12**, 009 (2022).
- [18] A. Altland, M. Buchhold, S. Diehl, and T. Micklitz, Dynamics of measured many-body quantum chaotic systems, *Phys. Rev. Res.* **4**, L022066 (2022).
- [19] Y. Fuji and Y. Ashida, Measurement-induced quantum criticality under continuous monitoring, *Phys. Rev. B* **102**, 054302 (2020).
- [20] S.-K. Jian, Z.-C. Yang, Z. Bi, and X. Chen, Yang-Lee edge singularity triggered entanglement transition, *Phys. Rev. B* **104**, L161107 (2021).
- [21] G. S. Bentsen, S. Sahu, and B. Swingle, Measurement-induced purification in large- N hybrid Brownian circuits, *Phys. Rev. B* **104**, 094304 (2021).
- [22] Z.-C. Yang, Y. Li, M. P. A. Fisher, and X. Chen, Entanglement phase transitions in random stabilizer tensor networks, *Phys. Rev. B* **105**, 104306 (2022).
- [23] R. Medina, R. Vasseur, and M. Serbyn, Entanglement transitions from restricted Boltzmann machines, *Phys. Rev. B* **104**, 104205 (2021).
- [24] O. Lunt and A. Pal, Measurement-induced entanglement transitions in many-body localized systems, *Phys. Rev. Res.* **2**, 043072 (2020).
- [25] M. Szyniszewski, A. Romito, and H. Schomerus, Entanglement transition from variable-strength weak measurements, *Phys. Rev. B* **100**, 064204 (2019).
- [26] Q. Tang and W. Zhu, Measurement-induced phase transition: A case study in the nonintegrable model by density-matrix renormalization group calculations, *Phys. Rev. Res.* **2**, 013022 (2020).
- [27] T. Iadecola, S. Ganeshan, J. H. Pixley, and J. H. Wilson, Dynamical entanglement transition in the probabilistic control of chaos, [arXiv:2207.12415](https://arxiv.org/abs/2207.12415) [cond-mat.dis-nn].
- [28] N. O’Dea, A. Morningstar, S. Gopalakrishnan, and V. Khemani, Entanglement and absorbing-state transitions in interactive quantum dynamics, *Phys. Rev. B* **109**, L020304 (2024).
- [29] V. Ravindranath, Y. Han, Z.-C. Yang, and X. Chen, Entanglement steering in adaptive circuits with feedback, *Phys. Rev. B* **108**, L041103 (2023).
- [30] P. Sierant and X. Turkeshi, Controlling entanglement at absorbing state phase transitions in random circuits, *Phys. Rev. Lett.* **130**, 120402 (2023).
- [31] P. Sierant and X. Turkeshi, Entanglement and absorbing state transitions in $(d + 1)$ -dimensional stabilizer circuits, *Chaos* **144**, 415 (2023).
- [32] M. Buchhold, T. Müller, and S. Diehl, Revealing measurement-induced phase transitions by pre-selection, [arXiv:2208.10506](https://arxiv.org/abs/2208.10506) [cond-mat.dis-nn].
- [33] S. Vijay, Measurement-driven phase transition within a volume-law entangled phase, [arXiv:2005.03052](https://arxiv.org/abs/2005.03052) [quant-ph].
- [34] R. Fan, S. Vijay, A. Vishwanath, and Y.-Z. You, Self-organized error correction in random unitary circuits with measurement, *Phys. Rev. B* **103**, 174309 (2021).
- [35] Y. Li, X. Chen, A. W. W. Ludwig, and M. P. A. Fisher, Conformal invariance and quantum nonlocality in critical hybrid circuits, *Phys. Rev. B* **104**, 104305 (2021).
- [36] M. Ippoliti, M. J. Gullans, S. Gopalakrishnan, D. A. Huse, and V. Khemani, Entanglement phase transitions in measurement-only dynamics, *Phys. Rev. X* **11**, 011030 (2021).
- [37] K. Klocke and M. Buchhold, Topological order and entanglement dynamics in the measurement-only XZZX quantum code, *Phys. Rev. B* **106**, 104307 (2022).
- [38] K. Klocke and M. Buchhold, Majorana loop models for measurement-only quantum circuits, *Phys. Rev. X* **13**, 041028 (2023).
- [39] Y. Li and M. P. A. Fisher, Decodable hybrid dynamics of open quantum systems with \mathbb{Z}_2 symmetry, *Phys. Rev. B* **108**, 214302 (2023).
- [40] Y. Li, R. Vasseur, M. P. A. Fisher, and A. W. W. Ludwig, Statistical mechanics model for Clifford random tensor networks and monitored quantum circuits, *Phys. Rev. B* **109**, 174307 (2024).
- [41] Y. Li, S. Vijay, and M. P. A. Fisher, Entanglement domain walls in monitored quantum circuits and the directed polymer in a random environment, *PRX Quantum* **4**, 010331 (2023).
- [42] Y. Li and M. P. A. Fisher, Statistical mechanics of quantum error correcting codes, *Phys. Rev. B* **103**, 104306 (2021).
- [43] X. Feng, B. Skinner, and A. Nahum, Measurement-induced phase transitions on dynamical quantum trees, *PRX Quantum* **4**, 030333 (2023).
- [44] F. Barratt, U. Agrawal, A. C. Potter, S. Gopalakrishnan, and R. Vasseur, Transitions in the learnability of global charges from local measurements, *Phys. Rev. Lett.* **129**, 200602 (2022).
- [45] A. Zabalo, M. J. Gullans, J. H. Wilson, R. Vasseur, A. W. W. Ludwig, S. Gopalakrishnan, D. A. Huse, and J. H. Pixley, Operator scaling dimensions and multifractality at measurement-induced transitions, *Phys. Rev. Lett.* **128**, 050602 (2022).
- [46] A. Zabalo, M. J. Gullans, J. H. Wilson, S. Gopalakrishnan, D. A. Huse, and J. H. Pixley, Critical properties of the measurement-induced transition in random quantum circuits, *Phys. Rev. B* **101**, 060301(R) (2020).
- [47] P. Sierant and X. Turkeshi, Universal behavior beyond multifractality of wave functions at measurement-induced phase transitions, *Phys. Rev. Lett.* **128**, 130605 (2022).
- [48] J. Iaconis, A. Lucas, and X. Chen, Measurement-induced phase transitions in quantum automaton circuits, *Phys. Rev. B* **102**, 224311 (2020).
- [49] Y. Han and X. Chen, Measurement-induced criticality in \mathbb{Z}_2 -symmetric quantum automaton circuits, *Phys. Rev. B* **105**, 064306 (2022).
- [50] H. Liu, T. Zhou, and X. Chen, Measurement-induced entanglement transition in a two-dimensional shallow circuit, *Phys. Rev. B* **106**, 144311 (2022).

- [51] S. Sang, Y. Li, T. Zhou, X. Chen, T. H. Hsieh, and M. P. A. Fisher, Entanglement negativity at measurement-induced criticality, *PRX Quantum* **2**, 030313 (2021).
- [52] Z. Weinstein, Y. Bao, and E. Altman, Measurement-induced power-law negativity in an open monitored quantum circuit, *Phys. Rev. Lett.* **129**, 080501 (2022).
- [53] X. Turkeshi, L. Piroli, and M. Schiró, Enhanced entanglement negativity in boundary-driven monitored fermionic chains, *Phys. Rev. B* **106**, 024304 (2022).
- [54] X. Turkeshi, L. Piroli, and M. Schiró, Density and current statistics in boundary-driven monitored fermionic chains, *Phys. Rev. B* **109**, 144306 (2024).
- [55] X. Turkeshi, R. Fazio, and M. Dalmonte, Measurement-induced criticality in $(2+1)$ -dimensional hybrid quantum circuits, *Phys. Rev. B* **102**, 014315 (2020).
- [56] X. Turkeshi, Measurement-induced criticality as a data-structure transition, *Phys. Rev. B* **106**, 144313 (2022).
- [57] P. Sierant, M. Schiró, M. Lewenstein, and X. Turkeshi, Measurement-induced phase transitions in $(d+1)$ -dimensional stabilizer circuits, *Phys. Rev. B* **106**, 214316 (2022).
- [58] A. Zabalo, J. H. Wilson, M. J. Gullans, R. Vasseur, S. Gopalakrishnan, D. A. Huse, and J. H. Pixley, Infinite-randomness criticality in monitored quantum dynamics with static disorder, *Phys. Rev. B* **107**, L220204 (2023).
- [59] P. W. Claeys, M. Henry, J. Vicary, and A. Lamacraft, Exact dynamics in dual-unitary quantum circuits with projective measurements, *Phys. Rev. Res.* **4**, 043212 (2022).
- [60] R. Morral-Yepes, F. Pollmann, and I. Lovas, Detecting and stabilizing measurement-induced symmetry-protected topological phases in generalized cluster models, *Phys. Rev. B* **108**, 224304 (2023).
- [61] G. Kells, D. Meidan, and A. Romito, Topological transitions in weakly monitored free fermions, *SciPost Phys.* **14**, 031 (2023).
- [62] A. Biella and M. Schiró, Many-body quantum Zeno effect and measurement-induced subradiance transition, *Quantum* **5**, 528 (2021).
- [63] X. Turkeshi, A. Biella, R. Fazio, M. Dalmonte, and M. Schiró, Measurement-induced entanglement transitions in the quantum Ising chain: From infinite to zero clicks, *Phys. Rev. B* **103**, 224210 (2021).
- [64] J. C. Hoke *et al.* (Google Quantum AI and Collaborators), Measurement-induced entanglement and teleportation on a noisy quantum processor, *Nature (London)* **622**, 481 (2023).
- [65] S. J. Garratt and E. Altman, Probing post-measurement entanglement without post-selection, *PRX Quantum* **5**, 030311 (2024).
- [66] E. V. H. Doggen, Y. Gefen, I. V. Gornyi, A. D. Mirlin, and D. G. Polyakov, Generalized quantum measurements with matrix product states: Entanglement phase transition and clusterization, *Phys. Rev. Res.* **4**, 023146 (2022).
- [67] E. V. H. Doggen, Y. Gefen, I. V. Gornyi, A. D. Mirlin, and D. G. Polyakov, Evolution of many-body systems under ancilla quantum measurements, *Phys. Rev. B* **107**, 214203 (2023).
- [68] I. Poboiko, P. Pöpperl, I. V. Gornyi, and A. D. Mirlin, Theory of free fermions under random projective measurements, *Phys. Rev. X* **13**, 041046 (2023).
- [69] E. V. H. Doggen, I. V. Gornyi, and A. D. Mirlin, Ancilla quantum measurements on interacting chains: Sensitivity of entanglement dynamics to the type and concentration of detectors, *Phys. Rev. B* **109**, 224203 (2024).
- [70] I. Poboiko, I. V. Gornyi, and A. D. Mirlin, Measurement-induced phase transition for free fermions above one dimension, *Phys. Rev. Lett.* **132**, 110403 (2024).
- [71] F. Azad, A. Hallam, J. Morley, and A. G. Green, Phase transitions in the classical simulability of open quantum systems, *Sci. Rep.* **13**, 8866 (2023).
- [72] M. Kolodrubetz, Optimality of Lindblad unfolding in measurement phase transitions, *Phys. Rev. B* **107**, L140301 (2023).
- [73] Z. Cheng and M. Ippoliti, Efficient sampling of noisy shallow circuits via monitored unraveling, *PRX Quantum* **4**, 040326 (2023).
- [74] D. Perez-Garcia, F. Verstraete, M. M. Wolf, and J. I. Cirac, Matrix product state representations, *Quantum Inf. Comput.* **7**, 401 (2007).
- [75] F. Verstraete, V. Murg, and J. I. Cirac, Matrix product states, projected entangled pair states, and variational renormalization group methods for quantum spin systems, *Adv. Phys.* **57**, 143 (2008).
- [76] F. Verstraete and J. I. Cirac, Matrix product states represent ground states faithfully, *Phys. Rev. B* **73**, 094423 (2006).
- [77] J. Haegeman, C. Lubich, I. Oseledets, B. Vandereycken, and F. Verstraete, Unifying time evolution and optimization with matrix product states, *Phys. Rev. B* **94**, 165116 (2016).
- [78] J. Haegeman, T. J. Osborne, and F. Verstraete, Post-matrix product state methods: To tangent space and beyond, *Phys. Rev. B* **88**, 075133 (2013).
- [79] E. Leviatan, F. Pollmann, J. H. Bardarson, D. A. Huse, and E. Altman, Quantum thermalization dynamics with matrix-product states, [arXiv:1702.08894](https://arxiv.org/abs/1702.08894) [cond-mat.stat-mech].
- [80] B. Kloss, Y. Bar Lev, and D. Reichman, Time-dependent variational principle in matrix-product state manifolds: Pitfalls and potential, *Phys. Rev. B* **97**, 024307 (2018).
- [81] A. Hallam, J. G. Morley, and A. G. Green, The Lyapunov spectra of quantum thermalisation, *Nat. Commun.* **10**, 075133 (2019).
- [82] M. Medenjak and J. De Nardis, Domain wall melting in spin-1 XXZ chains, *Phys. Rev. B* **101**, 081411(R) (2020).
- [83] F. Pollmann, S. Mukerjee, A. M. Turner, and J. E. Moore, Theory of finite-entanglement scaling at one-dimensional quantum critical points, *Phys. Rev. Lett.* **102**, 255701 (2009).
- [84] L. Tagliacozzo, T. R. de Oliveira, S. Iblisdir, and J. I. Latorre, Scaling of entanglement support for matrix product states, *Phys. Rev. B* **78**, 024410 (2008).
- [85] B. Vanhecke, J. Hasik, F. Verstraete, and L. Vanderstraeten, Scaling hypothesis for projected entangled-pair states, *Phys. Rev. Lett.* **129**, 200601 (2022).
- [86] B. Vanhecke, J. Haegeman, K. Van Acoleyen, L. Vanderstraeten, and F. Verstraete, Scaling hypothesis for matrix product states, *Phys. Rev. Lett.* **123**, 250604 (2019).
- [87] U. Agrawal, A. Zabalo, K. Chen, J. H. Wilson, A. C. Potter, J. H. Pixley, S. Gopalakrishnan, and R. Vasseur, Entanglement and charge-sharpening transitions in $U(1)$ symmetric monitored quantum circuits, *Phys. Rev. X* **12**, 041002 (2022).
- [88] U. Agrawal, J. Lopez-Piqueres, R. Vasseur, S. Gopalakrishnan, and A. C. Potter, Observing quantum

- measurement collapse as a learnability phase transition, [arXiv:2311.00058](https://arxiv.org/abs/2311.00058).
- [89] F. Barratt, U. Agrawal, S. Gopalakrishnan, D. A. Huse, R. Vasseur, and A. C. Potter, Field theory of charge sharpening in symmetric monitored quantum circuits, *Phys. Rev. Lett.* **129**, 120604 (2022).
- [90] H. Oshima and Y. Fuji, Charge fluctuation and charge-resolved entanglement in a monitored quantum circuit with $U(1)$ symmetry, *Phys. Rev. B* **107**, 014308 (2023).
- [91] J. F. Wienand, S. Karch, A. Impertro, C. Schweizer, E. McCulloch, R. Vasseur, S. Gopalakrishnan, M. Aidelsburger, and I. Bloch, Emergence of fluctuating hydrodynamics in chaotic quantum systems, [arXiv:2306.11457](https://arxiv.org/abs/2306.11457) [cond-mat.quant-gas].
- [92] E. McCulloch, J. De Nardis, S. Gopalakrishnan, and R. Vasseur, Full counting statistics of charge in chaotic many-body quantum systems, *Phys. Rev. Lett.* **131**, 210402 (2023).
- [93] G. Cecile, J. De Nardis, and E. Ilievski, Squeezed ensembles and anomalous dynamic roughening in interacting integrable chains, *Phys. Rev. Lett.* **132**, 130401 (2024).
- [94] L. Lumia, E. Tirrito, R. Fazio, and M. Collura, Measurement-induced transitions beyond Gaussianity: A single particle description, *Phys. Rev. Res.* **6**, 023176 (2024).
- [95] B. Xing, X. Turkeshi, M. Schiró, R. Fazio, and D. Poletti, Interactions and integrability in weakly monitored Hamiltonian systems, *Phys. Rev. B* **109**, L060302 (2024).
- [96] K. Jacobs and D. A. Steck, A straightforward introduction to continuous quantum measurement, *Contemp. Phys.* **47**, 279 (2006).
- [97] H. M. Wiseman and G. J. Milburn, *Quantum Measurement and Control* (Cambridge University Press, Cambridge, UK, 2009).
- [98] A. Barchielli and M. Gregoratti, *Quantum Trajectories and Measurements in Continuous Time* (Springer, Berlin, Heidelberg, 2009).
- [99] G. Vidal, Efficient classical simulation of slightly entangled quantum computations, *Phys. Rev. Lett.* **91**, 147902 (2003).
- [100] C. Hubig, J. Haegeman, and U. Schollwöck, Error estimates for extrapolations with matrix-product states, *Phys. Rev. B* **97**, 045125 (2018).
- [101] S. R. White, Minimally entangled typical quantum states at finite temperature, *Phys. Rev. Lett.* **102**, 190601 (2009).
- [102] A. Iwaki, A. Shimizu, and C. Hotta, Thermal pure quantum matrix product states recovering a volume law entanglement, *Phys. Rev. Res.* **3**, L022015 (2021).
- [103] A. A. Michailidis, C. J. Turner, Z. Papić, D. A. Abanin, and M. Serbyn, Slow quantum thermalization and many-body revivals from mixed phase space, *Phys. Rev. X* **10**, 011055 (2020).
- [104] M. Ljubotina, B. Roos, D. A. Abanin, and M. Serbyn, Optimal steering of matrix product states and quantum many-body scars, *PRX Quantum* **3**, 030343 (2022).
- [105] J. M. Koh, S.-N. Sun, M. Motta, and A. J. Minnich, Measurement-induced entanglement phase transition on a superconducting quantum processor with mid-circuit readout, *Nat. Phys.* **19**, 1314 (2023).
- [106] Y. Li, Y. Zou, P. Glorioso, E. Altman, and M. P. A. Fisher, Cross entropy benchmark for measurement-induced phase transitions, *Phys. Rev. Lett.* **130**, 220404 (2023).
- [107] M. Fishman, S. R. White, and E. M. Stoudenmire, Codebase release 0.3 for ITensor, *SciPost Phys. Codebases* **4** (2022).
- [108] A. W. Sandvik, Computational studies of quantum spin systems, *AIP Conf. Proc.* **1297**, 135 (2010).
- [109] N. Kawashima and N. Ito, Critical behavior of the three-dimensional $\pm J$ model in a magnetic field, *J. Phys. Soc. Jpn.* **62**, 435 (1993).
- [110] H. Lóio, A. De Luca, J. De Nardis, and X. Turkeshi, Purification timescales in monitored fermions, *Phys. Rev. B* **108**, L020306 (2023).